Microfabrication and Integration of Diazonium-Based Aromatic Molecular Junctions

Jie Ru,[†,‡] Bryan Szeto,[†] Andrew Bonifas,[†,§] and Richard L. McCreery*,[†,‡]

National Institute for Nanotechnology, National Research Council Canada, Edmonton, Alberta T6G 2M9, Canada, Department of Chemistry, University of Alberta, Edmonton, Alberta T6G 2R3, Canada, and Department of Materials Science and Engineering, The Ohio State University, Columbus, Ohio 43210, United States

ARTICLE

ABSTRACT Microfabrication techniques common in commercial semiconductor manufacturing were used to produce carbon/nitroazobenzene/Cu/Au molecular junctions with a range of areas from 3 × 3 to 400 × 400 μm, starting with 100-mm-diameter silicon wafers. The approach exhibited high yield (90−100%) and excellent reproducibility of the current density (relative standard deviation of typically 15%) and 32 devices on a chip. Electron-beam-deposited carbon films are introduced as substrates and may be applied at the full wafer level before dicing and electrochemical deposition of the molecular layer. The current scaled with the device area over a factor of >600, and the current density was quantitatively consistent with structurally similar molecular junctions made by other techniques. The current densities were weakly dependent on temperature over the range of 100−390 K, and maximum current densities above 400 A/cm^2 were observed without breakdown. To simulate processing and operation conditions, the junction stability was tested at elevated temperatures. The *JV* curves of microfabricated junctions were unchanged after 22 h at 100 °C. A ~50% increase in the current density was observed after 20 h at 150 °C but then remained constant for an additional 24 h. Parallel fabrication, thermal stability, and high yield are required for practical applications of molecular electronics, and the reported results provide important steps toward integration of molecular electronic devices with commercial processes and devices.

KEYWORDS: microelectronics • molecular electronics • microfabrication • carbon materials • molecular junction • electron transport

INTRODUCTION

Academic and commercial interest in molecular electronics is driven by the prospect of novel device functionalities and higher device density, which are potentially available when molecules are incorporated into microelectronic devices as active circuit components (1−9). Phenomena such as conductance switching (10−17), negative differential resistance (18−20), rectification (21, 22), and quantum mechanical tunneling (23−28) have been observed in molecular electronic devices and have potentially significant applications in microelectronics. One likely commercial manifestation of molecular electronics involves “hybrid” circuits, which combine the highly refined fabrication techniques of the conventional semiconductor industry with molecular components that enhance function, such as memory devices, photonics, and chemical sensors. The hybrid approach maintains the cost-effective, massively parallel processing of the complementary metal−oxide semiconductor (CMOS) industry but adds new molecule-based electronic behavior and functions (29, 30). For a hybrid approach to be practical, the molecular components must be compatible with CMOS in terms of fabrication and operating temperatures, substrate materials, and fabrication steps such as vapor deposition and photolithography while exhibiting high device yield and reproducible electronic behavior. Such compatibility has been explored for molecular junctions based on Au/self-assembled monolayer/conducting polymer architecture for the case of alkane (di)thiol molecular components (31, 32). Full wafer (150-mm-diameter) fabrication of 20 000 junctions with high yield was demonstrated, allowing basic logic circuits to be fabricated from molecular components. While these papers represent significant progress toward integration with commercial microelectronics, the conducting polymer used for the “top contact” is not a common material in semiconductor processing, and the finished devices degraded at temperatures above 50 °C (33). The authors conclude that “The upper limit of 50 °C is a strong limitation for the applicability of molecular electronics.”

Our laboratory has reported extensively on a different molecular junction paradigm, based on irreversible bonding of molecules to conducting carbon substrates via the reduction of aromatic diazonium reagents (29, 34−36). The molecule−substrate bond is strong (~4 eV) and stable to >500 °C (37, 38), and the Cu/Au top contact is applied by conventional electron-beam deposition. Comparison of the “direct” e-beam deposition to an “indirect” technique based on surface diffusion of remotely deposited Cu confirmed that Cu does not significantly penetrate the molecular layer (34).

* Corresponding author. E-mail: mccreery@ualberta.ca.
Received for review September 3, 2010 and accepted November 3, 2010
[†] National Research Council Canada.
[‡] University of Alberta.
[§] The Ohio State University.
DOI: 10.1021/am100833e
2010 American Chemical Society

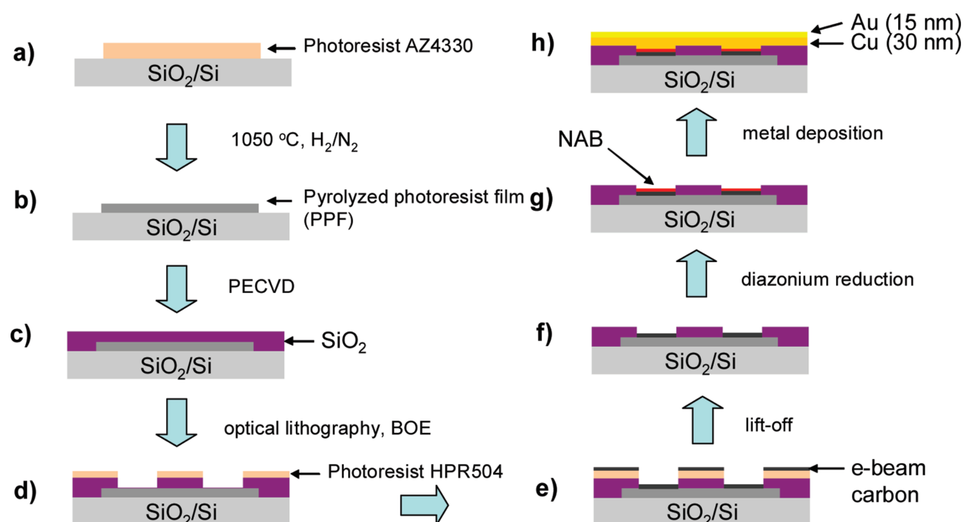

FIGURE 1. Process flowchart for the fabrication of microfabricated carbon/molecule/metal junctions. See the text and Supporting Information for details.

Electronic phenomena observed in such devices include nonlinear *JV* curves controlled by tunneling (29, 34, 39, 40), rectification (41), conductance switching in molecules and polymers (41−43), low-volatility memory based on TiO_2 redox events (44−46), and reversible formation of metal filaments (47). Our previous investigations were based on relatively large (100 × 100 to 500 × 500 μm) junctions made with "benchtop" photolithography and resulted in devices with excellent cycle life (>10^9 voltage cycles to ∼1 mA peak current) and temperature stability over a 5−450 K range (39). The current work was undertaken to determine if similar aromatic molecular junctions could be microfabricated in parallel using photolithography in a size range from 3 × 3 to 400 × 400 μm and to explore e-beam-deposited carbon as an alternative to the pyrolyzed photoresist film (PPF) used previously. In addition to achieving excellent device yield and reproducibility, microfabricated aromatic junctions scaled with an area over a factor of at least 600 and had electronic characteristics very similar to those of the large junctions reported previously. We used carbon/nitroazobenzene (NAB)/Cu/Au devices for microfabrication because their electronic properties were well established, with an exponential dependence of the current on bias and the molecular layer thickness consistent with that of quantum mechanical tunneling (34, 35, 39). In addition, the relatively large areas of previous carbon/NAB/Cu molecular junctions permitted spectroscopic confirmation of the device structure, as well as dynamics under bias (46, 48, 49). Such devices may be useful as "varistors" in voltage limiting circuits, but our main emphasis here is demonstration of microfabrication and tolerance of the processing conditions. The parallel fabrication and device structure described below should be broadly applicable to a variety of two-terminal devices with different functions.

EXPERIMENTAL SECTION

Junction fabrication procedures and materials are described in detail in the Supporting Information and shown schematically in the flowchart of Figure 1. Briefly, the steps are as follows, labeled as indicated in Figure 1: (a) photoresist AZ P4330-RS was spin-coated and patterned using standard optical lithography; (b) pyrolysis of the photoresist in forming gas (95% N_2 + 5% H_2) at 1050 °C resulted in a conductive amorphous carbon substrate (PPF); (c) a SiO_2 layer (300 nm) was deposited as an insulating layer using plasma-enhanced chemical vapor deposition (PECVD); (d) vertical junction holes were defined in the PECVD SiO_2 layer by optical lithography and buffered oxide etching; (e) wafers were diced and then e-beam evaporation of a 10 nm carbon film ("e-carbon") occurred; (f) the photoresist used in step d was stripped by rinsing with acetone; (g) the molecular layer was covalently attached to the carbon surface in the junction holes using electrochemical methods; (h) the junction was completed by consecutive e-beam depositions of Cu (30 nm) and Au (15 nm) through a shadow mask to form the top electronic contacts, with an initial chamber pressure of ∼2×10^{-6} Torr, increasing during deposition to $(3-10) \times 10^{-6}$ Torr. Junction areas are stated by their nominal dimensions (e.g., 16 × 16 μm), but the junction areas were individually determined with optical microscopy or scanning electron microscopy (SEM), as listed in Table 1. Both PPF (35, 36, 50, 51) and e-carbon have been described previously (52, 53) and exhibit metallic behavior resistivities of about 0.006 Ω-cm (PPF) and 0.015 Ω-cm (e-carbon). As is apparent from Figure 2A, each chip had 3 rows of 11 junctions with one "blank" having no aperture for NAB deposition, yielding 32 usable devices on each sample chip.

Table 1. Comparison of PPF/e-Carbon/NAB(3.8)/Cu Junctions with Varying Area

dimensions (μm)	area (μm^2)[a]	yield[b]	*I* at 0.5 V (A)	*J* at 0.5 V (A/cm^2)	rsd (%)
400 × 400	156000	9/9	5.11×10^{-4}	0.325	24.2
180 × 180	31000	10/10	9.94×10^{-5}	0.321	24.9
80 × 80	6400	10/10	1.07×10^{-5}	0.173	10.6
35 × 35	1300	10/10	2.16×10^{-6}	0.173	18.8
16 × 16	250	10/10	4.04×10^{-7}	0.162	11.6
7 × 7	50	10/10	7.27×10^{-8}	0.145	87.2
3 × 3	10	8/10	3.95×10^{-9}	0.040	106.6

[a] Determined with optical microscopy or SEM of completed junctions. [b] Number of devices that did not exhibit high linear currents characteristic of direct C/Cu contact.

Unless stated otherwise, current density/voltage (*JV*) curves were obtained at 1 V/s in three-wire mode, to correct for contact

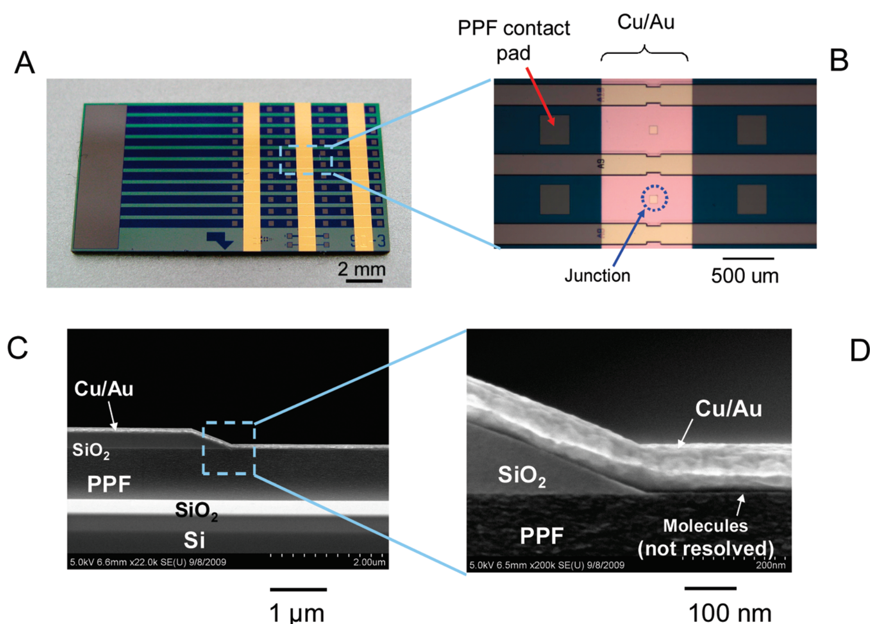

FIGURE 2. (A) Image of a diced sample showing three rows of molecular junctions. The large pad on the left allowed electronic contact to each bottom contact during molecular layer formation but was cleaved off after electrochemical diazonium reduction and metal deposition. (B) Close-up of the junction region, showing metal top contact. (C) SEM cross section of the sample cleaved through the junction region. (D) Magnified view of part C.

and lead resistance. "Yield" indicates the percentage of junctions that did not show high currents characteristic of metal penetration (i.e., "shorts"), while the reproducibility is stated as the relative standard deviation (rsd) of the current density at $V = 0.5$ V for nonshorted junctions of the same type. Junctions are designated with the materials involved, and the molecular layer thickness in nanometers was determined from atomic force microscopy (AFM) "scratching" (54) of microfabricated devices without Cu/Au top contacts. For example, PPF/NAB(4.5)/Cu indicates a 4.5-nm-thick multilayer of NAB on a PPF substrate. Additional experimental details for X-ray photoelectron microscopy (XPS), AFM, and SEM analyses are provided in the Supporting Information.

RESULTS

As described above, the PPF substrates were fabricated on full 100 mm wafers, and all lithography was completed before electrochemical deposition after step f in Figure 1. A diced sample after step h is shown in Figure 2A, with a sacrificial connector that permitted electrical contact to all 32 junction pads on one chip. This connector was used for electrochemical deposition from diazonium solutions and then cleaved off the chip after metal deposition to electronically isolate the individual junctions during electronic testing. It is certainly feasible to perform the electrochemical deposition at the full wafer level, but this was not attempted here because of the large wafer diameter. For example, Cu plating of full 200−300-mm-diameter wafers via the "Damascene" process is common in commercial semiconductor processing (55, 56), a procedure that is likely adaptable to molecular layer formation through diazonium reduction. As shown in Figure S1 in the Supporting Information, the e-carbon surface after all lithography steps but before diazonium reduction has a root-mean-square (rms) roughness of 0.42 nm, with the AFM image showing no observable defects. Freshly fabricated PPF before any microfabrication steps has an AFM roughness of 0.36 nm, indicating that no roughness was induced by the various lithography and etching steps. A magnified image of a finished junction is shown in Figure 2B, and SEM cross sections of cleaved junctions are shown in parts C and D of Figure 2. Contact pads visible on both sides of the junction permit access to the PPF with tungsten probes. The angled SiO_2 junction at the carbon substrate results from the buffered oxide etch and assures continuity of the Cu/Au contact across the transition from the molecular layer to SiO_2. Note that the molecular layer is too thin (2−5 nm) to observe at SEM magnification.

An overlay of all 32 current density/voltage curves (JV curves) for a PPF/NAB(3.8)/Cu sample is shown in Figure 3A, for the case of a 80 × 80 μm junction area. Although the yield was 100% (32/32) with no indication of direct PPF−Cu "shorts", the rsd of J at 0.5 V was 71%, implying significant junction variability. XPS analysis of the PPF surface (Figure S2 in the Supporting Information) showed that the atomic O/C ratio increased from 4.0% to 21.8% during microfabrication, likely because of the CVD plasma (step c in Figure 1). Surface oxides are likely to interfere with attachment of the molecular layer via diazonium reduction and may account for the variable behavior. To address this problem, a 10-nm-thick layer of disordered carbon was deposited by e-beam deposition (52) between steps d and e of Figure 1. The rms roughness was essentially unchanged by the e-carbon deposition, increasing from 0.36 to 0.42 nm (Figure S1 in the Supporting Information), and the O/C ratio was reduced from 21.8 to 6.8% (Figure S2 in the Supporting Information). As reported previously for silicon substrates, e-carbon deposition has a very small effect on the roughness of the underlying substrate material (52). Overlays of JV curves for all 32 PPF/e-carbon/NAB(4.5)/Cu junctions on one chip are shown in Figure 3B, and the same data set is shown

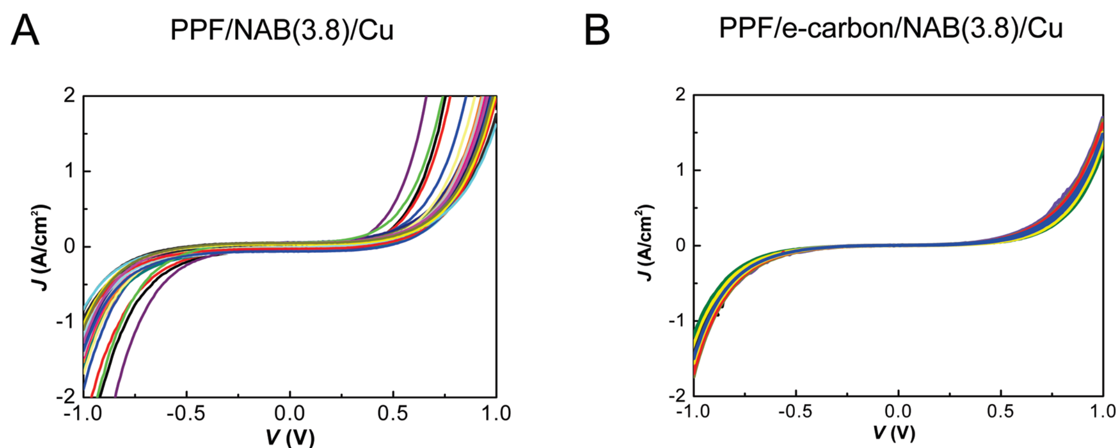

FIGURE 3. A total of 32 overlaid *JV* curves for molecular junctions with 3.8 nm thickness of NAB fabricated with the process of Figure 1 but without (A) and with (B) a 10 nm layer of e-beam-deposited carbon between the PPF and NAB layers. The device area was 80 × 80 μm. The yield for both data sets was 100% (32/32), and rsd for *J* (0.5 V) for data set B was 10%.

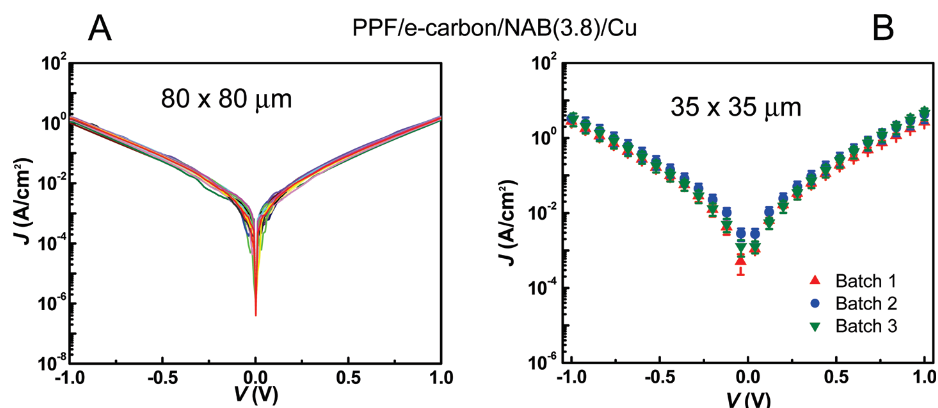

FIGURE 4. (A) Results of Figure 3B plotted on a log scale. (B) Average *JV* responses for three batches of 35 × 35 μm PPF/e-carbon/NAB(3.8)/Cu junctions made on different days on different wafers, with error bars shown for the ±1 standard deviation of 10 junctions in each batch.

on a logarithmic scale in Figure 4A. The yield remains 100%, but the addition of an e-carbon layer improves the rsd for *J* (0.5 V) to 10%, compared to 71% without the e-carbon film. As shown in Table S1 in the Supporting Information, the e-carbon layer improved the yield and reproducibility of junctions for all of the areas studied. The close similarity of the average *JV* curves in parts A and B of Figure 3 indicates that the e-carbon added negligible resistance to the PPF/NAB/Cu junction. Given the significant improvement in the reproducibility, the e-carbon layer was included in all subsequent experiments and figures. Wafer-to-wafer reproducibility was assessed by comparing junctions fabricated on three separate wafers, with the entire pyrolysis, lithography, NAB deposition, and metal deposition carried out independently and on different days. The mean *JV* curves for 10 junctions (35 × 35 μm for each wafer) are shown in Figure 4B, with error bars. The rsd for *J* (0.5 V) for a total of 29 junctions on three samples was 38%, with one apparent shorted junction.

JV curves from a range of junction areas from 16 × 16 to 400 × 400 μm are shown in Figure 5A, all for PPF/e-carbon/NAB(3.8)/Cu microfabricated junctions. As expected, the current decreases for smaller areas, with no apparent change in the curve shape or symmetry. When plotted as *JV* curves in Figure 5B, the five curves approximately coincide, indicating that the current scales with area over a range of factors of at least 600. Table 1 shows the numerical results for a wider range of junction dimensions, covering a factor of 2.5 × 10^4 in area, and Figure S3 in the Supporting Information shows current densities for nine junctions selected randomly for each area. There is no obvious trend in the current density with areas between 16 × 16 and 400 × 400 μm junctions or any significant change in the shape of the *JV* curves. SEM inspection of the junctions with different areas (shown in Figure S4 in the Supporting Information) reveals that the junction shape becomes rounded below 16 × 16 μm and debris or defects are apparent for the smaller sizes. It appears that the lower precision observed for 3 × 3 and 7 × 7 μm junctions is due, in part, to "edge effects" resulting from their larger edge/area ratio.

As described in detail previously (36, 54, 57−59), diazonium reduction may be used to produce molecular layers of varying thickness, by controlling the deposition conditions and verifying the layer thickness with AFM. Junctions were prepared with dimensions of 35 × 35 μm and NAB thicknesses from 2.2 to 5.2 nm, and their *JV* curves are plotted in Figure 6A. There is very little change in shape with the NAB thickness, while the conductance decreases by a factor of ~500 for the thickness range studied. The plot of ln *J* (0.1 V) shown in Figure 6B demonstrates the exponential dependence on the thickness, with a slope of 2.6 nm^{-1} at a bias of 0.1 V for the thickness range of 2.2−5.2 nm. Additional plots

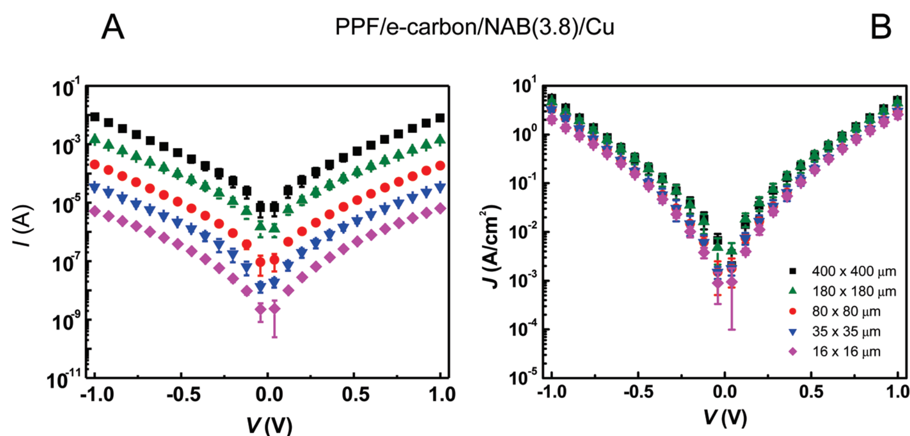

FIGURE 5. (A) Average current−voltage curves with ±1 standard deviation error bars for five junction areas. From bottom to top: 16 × 16, 35 × 35, 80 × 80, 180 × 180, and 400 × 400 μm. (B) Same curves as part A but plotted semilogarithmically in the current density.

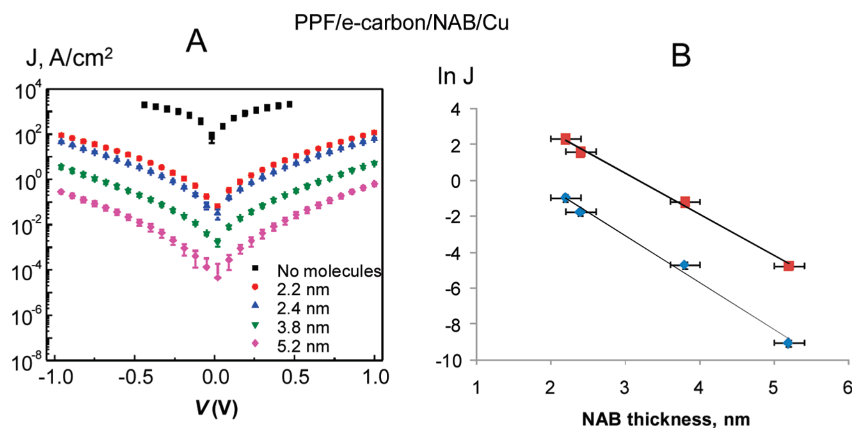

FIGURE 6. (A) JV curves for 35 × 35 μm molecular junctions with varying NAB thicknesses from bottom to top: 5.2, 3.8, 2.4, and 2.2 nm. The top curve is with NAB absent and represents a direct e-carbon to Cu contact. (B) Plot of ln J vs NAB thickness (nm) for $V = 0.1$ and 0.5 V.

at $V = 0.3$, 0.5, and 0.7 V are also linear, with slopes of 2.4, 2.3, and 2.2 nm^{-1}, respectively, indicating a small decrease in the attenuation coefficient (usually denoted as β) with increasing bias. Decreasing β with bias has been reported previously for diazonium-derived molecular junctions (39) and has been analyzed to elucidate a transport mechanism in alkanethiol devices (60).

Although the carbon surfaces used here (PPF and e-carbon) have the attractive property of forming strong surface bonds via diazonium chemistry, their conductivity is lower than that of most metals. Particularly for conduction through thin PPF "leads" of the molecular junctions, significant ohmic potential drops occur, leading to some distortion of the JV response. This error is effectively corrected by using the "three-wire" and "four-wire" measurement techniques, in which a "sense" probe is added to accurately monitor the junction voltage and correct for ohmic losses in the PPF and Cu leads. This effect is shown in Figure 7A for the case of a large (400 × 400 μm) NAB junction, where the mA currents result in significant ohmic losses through the lead and contact resistances in series with the molecular junction. The "three-wire" case has a sense lead on the PPF opposite the "drive" voltage, while the "four-wire" arrangement has an additional sense lead on the Cu/Au opposite the connection to the current amplifier (circuit details are shown in Figure S5 in the Supporting Information). Although the largest error is caused by the PPF conductivity, the Cu/Au lead also contributes for the large junctions. Reduction of the junction size to 16 × 16 μm greatly reduces the error, with only a small ohmic loss in the PPF. It is clear that lead resistance is a consideration in any practical devices containing PPF or e-carbon, but the problem becomes minor as the junction size decreases.

The temperature dependence of junction conductance was determined over the range of 100−300 K for NAB(3.8) and 100−390 K for NAB(5.2). Junctions could be reversibly cycled over this temperature range without observable changes in the JV behavior. The Arrhenius plots shown in Figure S6 in the Supporting Information indicate a weak temperature dependence over most of this range, with Arrhenius slopes of 1−6 meV for temperatures below 200 K and an increase in the slope to 20−40 meV between 250 and 390 K. This behavior is quite similar to that of our previously reported "cross junctions" made without microfabrication, which were studied over the temperature range of 5−450 K (35, 39). The temperature independence below 200 K was concluded to be due to tunneling transport through the highest occupied molecular orbital (HOMO), while the 20−40 meV Arrhenius slopes at higher temperature are consistent with broadening of the Fermi function

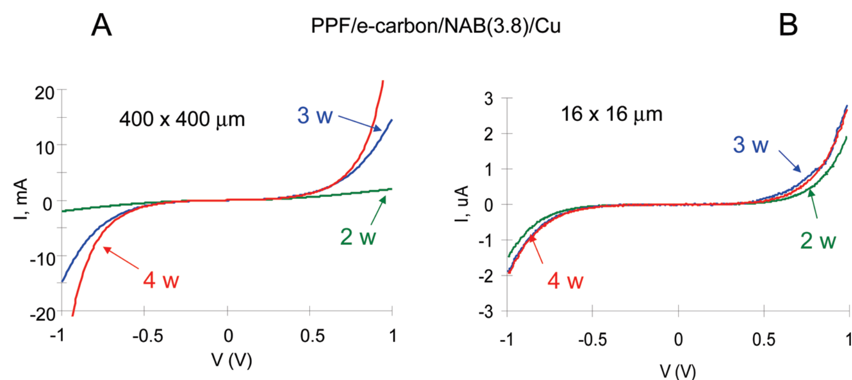

FIGURE 7. Effect of the contact and lead resistance on observed current−voltage curves for NAB(3.8) junctions of different sizes. Three-wire (3 w) geometry corrects for PPF resistance, while four-wire (4 w) corrects for both PPF and Cu/Au resistance. Note the large differences in the current scales.

in the contacts (39). Therefore, transport in the microfabricated junctions is consistent with a tunneling mechanism over the entire temperature range studied, with no indication of reorganization or molecular configuration changes. The thermal tolerance of carbon/NAB/Cu junctions with 180 × 180 μm areas was assessed by heating for prolonged periods, with periodic determination of the *JV* behavior. A total of 22 h at 100 °C in vacuum had no observable effect on the *JV* curves (obtained at room temperature). Heating in a vacuum at 150 °C caused a gradual increase in the current by ~50%, with no change in the shape after 20 h, at which point the current remained constant for at least another 24 h.

We demonstrated previously that PPF/NAB/Cu molecular junctions are stable for at least 10^9 voltage scans, which had peak current densities of ~0.5 A/cm^2 (~1 mA for a 0.002 cm^2 device) (39). Given the much smaller areas of the microfabricated junctions reported here, it was possible to subject the junctions to higher voltages and current densities than studied previously. Current densities of 1000 A/cm^2 (>2.5 mA) at +3 V did not cause any observable changes in the *JV* behavior for a 16 × 16 μm junction. A negative bias of −2 V produced a current density of ~400 A/cm^2, but more negative bias resulted in irreversible breakdown and very high currents. Breakdown always occurred more readily for negative bias, when Cu/Au is at positive potential. Breakdown for negative bias is likely due to oxidation of Cu to a mobile Cu^+ ion, which is driven by the applied field to the carbon surface where it is reduced to form a filament (47). Metal filament formation has been invoked to explain conductance switching and memory effects in a variety of devices (61−64), many of which contain Cu or Ag (47, 65−67). Such filaments can be a source of hysteresis and pronounced conductance changes, but these effects were only evident in microfabricated carbon/NAB/Cu devices for high current densities (>1000 A/cm^2) when the Cu/Au electrode was at high positive bias (>2 V). For scans between ±2 V, the devices showed no hysteresis or conductance changes for millions of cycles. Recent reports have also implicated graphitic structures in conductance switching, possibly mediated by nanomechanical effects (10, 68). As already stated, no evidence for such effects in the PPF or e-beam carbon was observed in the current devices for a −2 to +3 V bias range.

DISCUSSION

The microfabricated junctions reported here exhibit current/voltage behavior that is qualitatively very similar to that reported previously for larger carbon/molecule/Cu devices, with an exponential dependence of the current on voltage and a strong dependence on the thickness of the molecular layer (35, 39). Although Au is more commonly used in molecular junctions, it is prone to penetration into the molecular layer, in some cases ending up at the bottom of a Au/S self-assembled monolayer (4, 69−73). Cu interacts more strongly with aromatic molecules than Au and has a higher surface energy, which presumably decreases penetration (35, 39, 40). We showed recently that Cu deposited with a "soft" deposition technique based on the surface diffusion of metal atoms at room temperature produced junctions with behavior very similar to that of the direct e-beam deposition used here (34). Furthermore, the *JV* curves for Au and Cu deposited with the "soft" technique were very similar, with the Au current densities approximately a factor of 4 larger than those for Cu. We have shown previously that the current densities for carbon/molecule/Cu junctions depend somewhat on the backpressure during deposition, but they do not contain any observable copper oxide (35). The direct e-beam deposition of Cu on diazonium-derived molecular layers has the important advantage of compatibility with conventional semiconductor processing. As noted in the introduction, massively parallel fabrication with sometimes significant temperature excursions is necessary in most conventional microelectronic manufacturing. Furthermore, "direct" physical vapor deposition is quite common in the semiconductor industry.

The carbon substrate used here and in previous reports has two important properties: the ability to form strong C−C bonds through diazonium reduction and a flatness (~0.4 nm rms) comparable to or less than the thickness of the molecular layer. Pyrolysis of the photoresist to produce PPF is not likely to be feasible in a production environment, but the current results show that e-beam-deposited carbon is a suitable substrate that produces junctions very similar to

those made directly on PPF. Provided a conducting substrate is sufficiently flat, it should be possible to deposit a 10−50-nm-thick layer of e-carbon through a conventional lithography mask. For example, it may be possible to fabricate support electronics for a molecular device with conventional CMOS procedures and then to fabricate molecular junctions on conducting pads exposed on the top layer of the CMOS wafer. Widely used chemical−mechanical polishing procedures could then provide a substrate flat to <1 nm, for either e-carbon deposition or molecular bonding. Obviously, there are many issues to resolve before practical integration of carbon-based molecular junctions with conventional microelectronics, but direct e-beam deposition of both carbon substrates and metal top contacts is a useful step in the process.

Quantitative comparisons of *JV* curves for molecular junctions made in different laboratories have been difficult because of differences in paradigm, fabrication conditions, molecular structure, measurement techniques, etc. (29) For the case of carbon/NAB/Cu/Au junctions made via diazonium chemistry, we can compare the current results to those reported previously. Note that these results were obtained over a period of ∼3 years, using three separate thin film evaporator systems, with a wide range of device areas and with both "direct" and "soft" deposition, with the latter being based on surface diffusion of room temperature Cu atoms. The rsd's of the current densities for each fabrication technique within each batch of junctions were 10−30%, and yields were consistently above 90%. The various fabrication methods and junction geometries exhibited average J (1 V) values as follows: "cross junction" with direct Cu deposition (35), 1.06 A/cm^2; "soft" deposition by metal diffusion (34), 0.66 A/cm^2; direct Cu deposition (34), 0.78 A/cm^2; microfabricated (current density adjusted to 4.5 nm NAB using $\beta = 2.6$ nm^{-1}), 0.60 A/cm^2; direct Cu deposition (39), 2.7 A/cm^2. The variations between the various methods is a factor of 4.5, which is at least partially attributable to fabrication and measurement variables, such as deposition backpressure, junction age, and uncompensated resistance. As shown in Figure 7, the latter effect is significant for large junction areas, as was the case for most of the previous devices. The consistency of the device behavior for a wide range of fabrication procedures and junction areas supports the conclusion that "direct" vapor-deposited Cu is a reliable top contact for diazonium-derived molecular layers on carbon substrates.

The dependence of the current density on the molecular layer thickness is less subject to fabrication variables and should not depend on the area. The attenuation coefficient (β) of 2.6 nm^{-1} at $V = 0.1$ V (Figure 6) is very close to that reported recently for larger junctions (2.5 nm^{-1}, also at 0.1 V), and in both cases, this value decreased slightly for increasing bias. Furthermore, it is close to the value of 2.1 nm^{-1} reported for electron transfer through diazonium-derived monolayers on glassy carbon to redox-active molecules in an electrolyte solution (74) and 2.1−2.2 nm^{-1} observed for cross junctions containing biphenyl and nitrobiphenyl (40). We reported recently a detailed analysis of the factors governing the shapes and magnitude of *JV* curves in carbon/molecule/Cu molecular junctions, including the magnitude of β (39). Briefly, the curve shape, temperature dependence, and thickness dependence are all consistent with quantum mechanical tunneling of holes through a barrier represented by the difference between the Fermi level of the contacts and the HOMO energy of the molecular layer. β is significantly smaller than that observed for alkanes (∼9 nm^{-1}) because of the extensive electron delocalization in aromatic molecular layers as well as the smaller Fermi level/HOMO offset. Furthermore, electron delocalization results in a HOMO energy, dielectric constant, and effective carrier mass that depend strongly on the molecular layer thickness (39). An important conclusion of both the earlier and current results is the absence of an "activated" process, which is the origin of the weak temperature dependence. Therefore, transport occurs via tunneling through a low barrier (∼1.5 eV) between the contact Fermi levels and the HOMO. As the HOMO energy approaches that of the contact Fermi level, we expect that electron transport will become much more efficient. The Fermi levels of PPF and Cu are close to −5 eV relative to a vacuum, and a variety of molecules have HOMO energies close to −5 eV. Theory predicts that, for the "resonant" case corresponding to zero Fermi level/HOMO offset, β should approach zero (75, 76) and the device will behave essentially as a "molecular short circuit" with high conductance.

The ability to "tune" the properties of carbon/molecule/Cu/Au devices by varying the HOMO energy and layer thickness permits fabrication of a wide variety of nonlinear "resistors" with an exponential dependence of the current on bias. Such devices may be useful in voltage-limiting circuits and spike suppression, similar to "varistors" in current use. It should be noted, however, that tunneling is a nondissipative process, with minimal heat generation, and the conduction mechanism is fundamentally different from that of classical resistors. In principle, the carbon/NAB/Cu devices could conduct very large current densities without local heating and may find uses in high-density microelectronics where heat dissipation has become a significant problem.

SUMMARY

Massively parallel fabrication, high yield and reproducibility, and compatibility with semiconductor processing are essential before molecular electronic devices can be integrated with commercial microelectronics. The microfabricated molecular junctions reported here represent significant steps toward these objectives. The strong, conjugated C−C surface bond between the molecules and the carbon substrate imparts good thermal stability and is stable to metal deposition and a variety of chemical processing. Although the smallest devices reported here were 3 × 3 μm, the junction structure itself is amenable to much smaller dimensions. Vapor-deposited carbon substrates and metal contacts can be applied with evaporators currently used in the industry, and reduction of diazonium reagents may be implemented with equipment similar to the widely used

ARTICLE

copper deposition "damascene" process. Finally, diazonium-derived aromatic molecular junctions can be made with a wide variety of chemical structures, possibly enabling new electronic functions.

Acknowledgment. This work was supported by the Natural Sciences and Engineering Research Council of Canada, the National Research Council Canada, the University of Alberta, and the Alberta Ingenuity Fund. The National Institute for Nanotechnology is operated as a partnership between the National Research Council and the University of Alberta and is jointly funded by the Government of Canada, the Government of Alberta, and the University of Alberta.

Supporting Information Available: AFM images, XPS results, statistics on the junction yield and reproducibility, SEM images, wiring diagrams, Arrhenius plots, and a detailed fabrication procedure. This material is available free of charge via the Internet at http://pubs.acs.org.

REFERENCES AND NOTES

(1) Yaffe, O.; Scheres, L.; Puniredd, S. R.; Stein, N.; Biller, A.; Lavan, R. H.; Shpaisman, H.; Zuilhof, H.; Haick, H.; Cahen, D.; Vilan, A. *Nano Lett.* **2009**, *9*, 2390.
(2) Vilan, A.; Yaffe, O.; Biller, A.; Salomon, A.; Kahn, A.; Cahen, D. *Adv. Mater.* **2010**, *22*, 140.
(3) Chen, F.; Hihath, J.; Huang, Z.; Li, X.; Tao, N. J. *Annu. Rev. Phys. Chem.* **2007**, *58*, 535.
(4) Haick, H.; Cahen, D. *Acc. Chem. Res.* **2008**, *41*, 359.
(5) Akkerman, H. B.; De Boer, B. *J. Phys.: Condens. Matter* **2008**, *20*, 013001.
(6) Kronemeijer, A. J.; Akkerman, H. B.; Kudernac, T.; Wees, B. J. v.; Feringa, B. L.; Blom, P. W. M.; Boer, B. d. *Adv. Mater.* **2008**, *20*, 1467.
(7) Selzer, Y.; Allara, D. *Annu. Rev. Phys. Chem.* **2006**, *57*, 593.
(8) Akkerman, H. B.; Blom, P. W. M.; de Leeuw, D. M.; de Boer, B. *Nature* **2006**, *441*, 69.
(9) McCreery, R. *Chem. Mater.* **2004**, *16*, 4477.
(10) Li, Y.; Sinitskii, A.; Tour, J. M. *Nat. Mater.* **2008**, *7*, 966.
(11) Lörtscher, E.; Jacob, W. C.; James, T.; Riel, H. *Small* **2006**, *2*, 973.
(12) Lewis, P.; Inman, C.; Yao, Y.; Tour, J.; Hutchinson, J.; Weiss, P. *J. Am. Chem. Soc.* **2004**, *126*, 12214.
(13) He, J.; Fu, Q.; Lindsay, S.; Ciszek, J. W.; Tour, J. M. *J. Am. Chem. Soc.* **2006**, *128*, 14828.
(14) Pease, A. R.; Jeppesen, J. O.; Stoddart, J. F.; Luo, Y.; Collier, C. P.; Heath, J. R. *Acc. Chem. Res.* **2001**, *34*, 433.
(15) Yeganeh, S.; Galperin, M.; Ratner, M. A. *J. Am. Chem. Soc.* **2007**, *129*, 13313.
(16) Cai, L.; Cabassi, M. A.; Yoon, H.; Cabarcos, O. M.; McGuiness, C. L.; Flatt, A. K.; Allara, D. L.; Tour, J. M.; Mayer, T. S. *Nano Lett.* **2005**, *5*, 2365.
(17) Galperin, M.; Ratner, M. A.; Nitzan, A. *Nano Lett.* **2005**, *5*, 125.
(18) Chen, J.; Wang, W.; Reed, M. A.; Rawlett, A. M.; Price, D. W.; Tour, J. M. *Appl. Phys. Lett.* **2000**, *77*, 1224.
(19) Chen, L.; Hu, Z.; Zhao, A.; Wang, B.; Luo, Y.; Yang, J.; Hou, J. G. *Phys. Rev. Lett.* **2007**, *99*, 146803.
(20) Dinglasan, J. A. M.; Michael Bailey, M.; Jong, B.; Park, J. B.; Dhirani, A.-A. *J. Am. Chem. Soc.* **2004**, *126*, 6491.
(21) Honciuc, A.; Metzger, R. M.; Gong, A.; Spangler, C. W. *J. Am. Chem. Soc.* **2007**, *129*, 8310.
(22) Metzger, R. M. *Chem. Phys.* **2006**, *326*, 176.
(23) Selzer, Y.; Cai, L.; Cabassi, M.; Yao, Y.; Tour, J.; Mayer, T.; Allara, D. *Nano Lett.* **2005**, *5*, 61.
(24) Selzer, Y.; Cabassi, M. A.; Mayer, T. S.; Allara, D. L. *J. Am. Chem. Soc.* **2004**, *126*, 4052.
(25) Lindsay, S. M.; Ratner, M. A. *Adv. Mater.* **2007**, *19*, 23.
(26) Xue, Y.; Ratner, M. A. *Phys. Rev. B* **2003**, *68*, 115406.
(27) Frederiksen, T.; Munuera, C.; Ocal, C.; Brandbyge, M.; Paulsson, M.; Sanchez-Portal, D.; Arnau, A. *ACS Nano* **2009**, *3*, 2073.
(28) Chen, F.; Tao, N. J. *Acc. Chem. Res.* **2009**, *42*, 429.
(29) McCreery, R. L.; Bergren, A. J. *Adv. Mater.* **2009**, *21*, 4303.
(30) McCreery, R. *Electrochem. Soc. Interface* **2004**, *13*, 46.
(31) Van Hal, P. A.; Smits, E. C. P.; Geuns, T. C. T.; Akkerman, H. B.; De Brito, B. C.; Perissinotto, S.; Lanzani, G.; Kronemeijer, A. J.; Geskin, V.; Cornil, J.; Blom, P. W. M.; De Boer, B.; De Leeuw, D. M. *Nat. Nano* **2008**, *3*, 749.
(32) Smits, E. C. P.; Mathijssen, S. G. J.; van Hal, P. A.; Setayesh, S.; Geuns, T. C. T.; Mutsaers, K. A. H. A.; Cantatore, E.; Wondergem, H. J.; Werzer, O.; Resel, R.; Kemerink, M.; Kirchmeyer, S.; Muzafarov, A. M.; Ponomarenko, S. A.; de Boer, B.; Blom, P. W. M.; de Leeuw, D. M. *Nature* **2008**, *455*, 956.
(33) Akkerman, H. B.; Kronemeijer, A. J.; Harkema, J.; van Hal, P. A.; Smits, E. C. P.; de Leeuw, D. M.; Blom, P. W. M. *Org. Electron.* **2010**, *11*, 146.
(34) Bonifas, A. P.; McCreery, R. L. *Nat. Nano* **2010**, *5*, 612.
(35) Bergren, A. J.; Harris, K. D.; Deng, F.; McCreery, R. *J. Phys.: Condens. Matter* **2008**, *20*, 374117.
(36) McCreery, R.; Wu, J.; Kalakodimi, R. J. *Phys. Chem. Chem. Phys.* **2006**, *8*, 2572.
(37) Toupin, M.; Belanger, D. *J. Phys. Chem. C* **2007**, *111*, 5394.
(38) Kuo, T.-C. Raman Spectroscopy and Electrochemistry of Modified Carbon Surfaces. Ph.D. Thesis, The Ohio State University, Columbus, OH, 1999.
(39) Bergren, A. J.; McCreery, R. L.; Stoyanov, S. R.; Gusarov, S.; Kovalenko, A. *J. Phys. Chem. C* **2010**, *114*, 15806.
(40) Anariba, F.; Steach, J.; McCreery, R. *J. Phys. Chem. B* **2005**, *109*, 11163.
(41) McCreery, R. L.; Dieringer, J.; Solak, A. O.; Snyder, B.; Nowak, A.; McGovern, W. R.; DuVall, S. *J. Am. Chem. Soc.* **2003**, *125*, 10748.
(42) Barman, S.; Deng, F.; McCreery, R. *J. Am. Chem. Soc.* **2008**, *130*, 11073.
(43) Solak, A. O.; Ranganathan, S.; Itoh, T.; McCreery, R. L. *Electrochem. Solid State Lett.* **2002**, *5*, E43.
(44) Wu, J.; McCreery, R. L. *J. Electrochem. Soc.* **2009**, *156*, P29.
(45) Wu, J.; Mobley, K.; McCreery, R. *J. Chem. Phys.* **2007**, *126*, 24704.
(46) Nowak, A.; McCreery, R. *J. Am. Chem. Soc.* **2004**, *126*, 16621.
(47) Ssenyange, S.; Yan, H.; McCreery, R. L. *Langmuir* **2006**, *22*, 10689.
(48) Mahmoud, A. M.; Bergren, A. J.; McCreery, R. L. *Anal. Chem.* **2009**, *81*, 6972.
(49) Nowak, A. M.; McCreery, R. L. *Anal. Chem.* **2004**, *76*, 1089.
(50) Ranganathan, S.; McCreery, R. L. *Anal. Chem.* **2001**, *73*, 893.
(51) Ranganathan, S.; McCreery, R. L.; Majji, S. M.; Madou, M. *J. Electrochem. Soc.* **2000**, *147*, 277.
(52) Blackstock, J. J.; Rostami, A. A.; Nowak, A. M.; McCreery, R. L.; Freeman, M.; McDermott, M. T. *Anal. Chem.* **2004**, *76*, 2544.
(53) Mattson, J. S.; Smith, C. A. *Anal. Chem.* **1975**, *47*, 1122.
(54) Anariba, F.; DuVall, S. H.; McCreery, R. L. *Anal. Chem.* **2003**, *75*, 3837.
(55) Gimenez-Romero, D.; Garcia-Jareno, J. J.; Agrisuelas, J.; Gabrielli, C.; Perrot, H.; Vicente, F. *J. Phys. Chem. C* **2008**, *112*, 4275.
(56) Matsumura, Y.; Enomoto, Y.; Tsuruoka, T.; Akamatsu, K.; Nawafune, H. *Langmuir* **2010**, *26*, 12448.
(57) Solak, A. O.; Eichorst, L. R.; Clark, W. J.; McCreery, R. L. *Anal. Chem.* **2003**, *75*, 296.
(58) Kariuki, J. K.; McDermott, M. T. *Langmuir* **2001**, *17*, 5947.
(59) Kariuki, J. K.; McDermott, M. T. *Langmuir* **1999**, *15*, 6534.
(60) Wang, W.; Lee, T.; Reed, M. A. *Phys. Rev. B* **2003**, *68*, 035416.
(61) Waser, R.; Dittmann, R.; Staikov, G.; Szot, K. *Adv. Mater.* **2009**, *21*, 2632.
(62) Waser, R.; Aono, M. *Nat. Mater.* **2007**, *6*, 833.
(63) Lau, C. N.; Stewart, D. R.; Williams, R. S.; Bockrath, M. *Nano Lett.* **2004**, *4*, 569.
(64) Strachan, J. P.; Pickett, M. D.; Yang, J. J.; Aloni, S.; Kilcoyne, A. L. D.; Medeiros-Ribeiro, G.; Williams, R. S. *Adv. Mater.* **2010**, *22*, 3573.
(65) Gilbert, N. E.; Gopalan, C.; Kozicki, M. N. *Solid-State Electron.* **2005**, *49*, 1813.
(66) Mitkova, M.; Kozicki, M. N.; Kim, H. C.; Alford, T. L. *Thin Solid Films* **2004**, *449*, 248.
(67) Kozicki, M. N.; Mitkova, M.; Park, M.; Balakrishnan, M.; Gopalan, C. *Superlattices Microstruct.* **2003**, *34*, 459.

(68) Sinitskii, A.; Tour, J. M. *ACS Nano* **2009**, *3*, 2760.
(69) Haick, H.; Cahen, D. *Prog. Surf. Sci.* **2008**, *83*, 217.
(70) Zhu, Z.; Daniel, T. A.; Maitani, M.; Cabarcos, O. M.; Allara, D. L.; Winograd, N. *J. Am. Chem. Soc.* **2006**, *128*, 13710.
(71) Walker, A. V.; Tighe, T. B.; Cabarcos, O. M.; Reinard, M. D.; Haynie, B. C.; Uppili, S.; Winograd, N.; Allara, D. L. *J. Am. Chem. Soc.* **2004**, *126*, 3954.
(72) Metzger, R. Unimolecular Electronics. *Nano and Molecular Electronics Handbook*; CRC Press: Boca Raton, FL, 2007.
(73) Metzger, R. M.; Baldwin, J. W.; Shumate, W. J.; Peterson, I. R.; Mani, P.; Mankey, G. J.; Morris, T.; Szulczewski, G.; Bosi, S.; Prato, M.; Comito, A.; Rubin, Y. *J. Phys. Chem. B* **2003**, *107*, 1021.
(74) Yang, H.-H.; McCreery, R. L. *Anal. Chem.* **1999**, *71*, 4081.
(75) Mujica, V.; Kemp, M.; Ratner, M. A. *J. Chem. Phys.* **1994**, *101*, 6856.
(76) Mujica, V.; Kemp, M.; Ratner, M. A. *J. Chem. Phys.* **1994**, *101*, 6849.

AM100833E